Supporting Information

Efficient production of hydrogen from H_2S via electrolysis using $CoFeS_2$ catalyst

Mukesh Kumar and Tharamani C. Nagaiah*

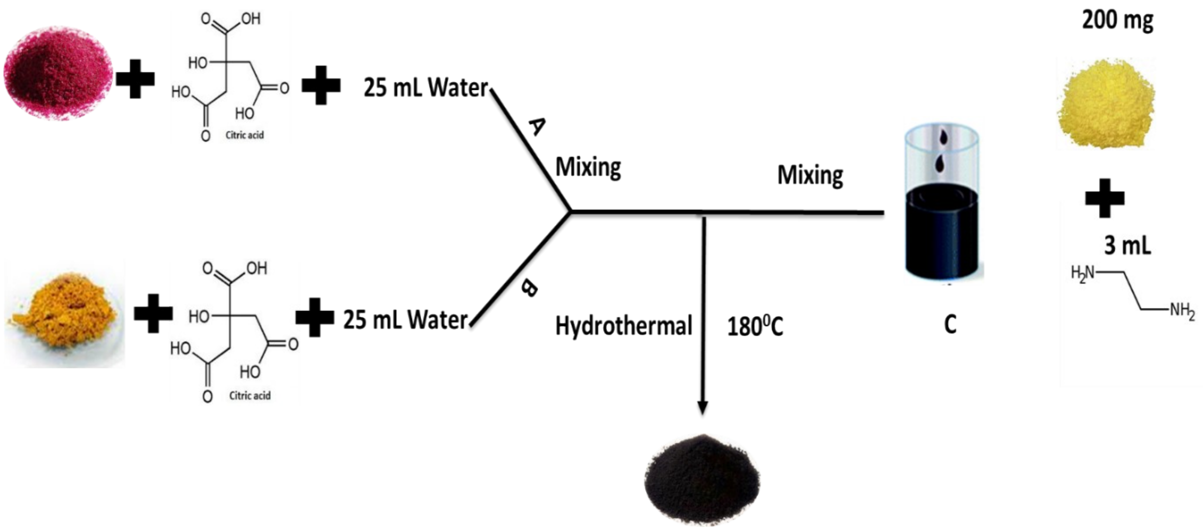

Fig. S1. Schematic representation for the synthesis of $CoFeS_2(x:y)$.

As shown in Fig. S2A, still yellow color unreacted sulfur based species were present in the remaining solution after the hydrothermal synthesis. So, if unreacted ethylene diamine (EDA) was present, it will show deep reddish brownish color instead of yellow color (Fig. S2B). From these observations, we get the idea that EDA was removed completely. Moreover, Citric acid 1750 g/L and EDA have very high solubilities in water, and unreacted precursors will immediately wash away with water. We have carefully washed the catalyst with a 1:1 water-ethanol mixture. As shown in Fig. S2A, the yellow color completely disappeared, increasing the no. of washing. We further monitored the electrolyte by UV and found that polysulfide peaks were completely removed.

And further, to reinsure that no sulfur is left, we have added EDA in this solution (after 7th wash). We noticed no color change (Fig. S2B), further confirming that the unreacted sulfur species are removed. Additionally, to ensure that S species are removed from the catalysts, we have deliberately added 100 mg of washed

$CoFeS_2$(3:1) in 6 mL of EDA and sonicated it for one hour. It is clear from Fig. S2C that there is no color change even after 24 h of standing, which further verifies that unreacted sulfur was removed entirely from the reaction mixture. Further, we did not get any citric acid in the solution by the acid-base titration, confirming all the elemental sulfur, EDA, and CA are removed, and the sample is pure.

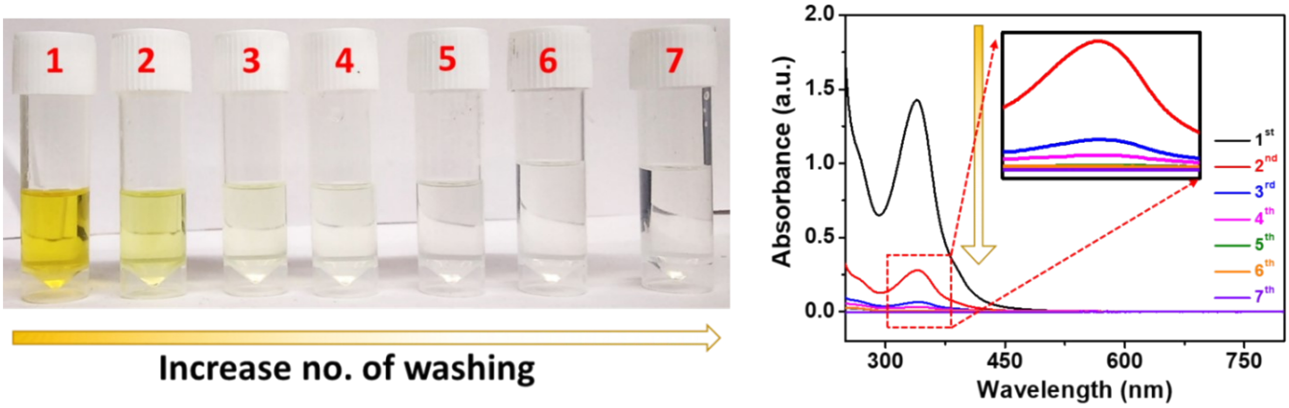

Fig. S2A. Photographs and corresponding UV of solvent retrieved after multiple washing.

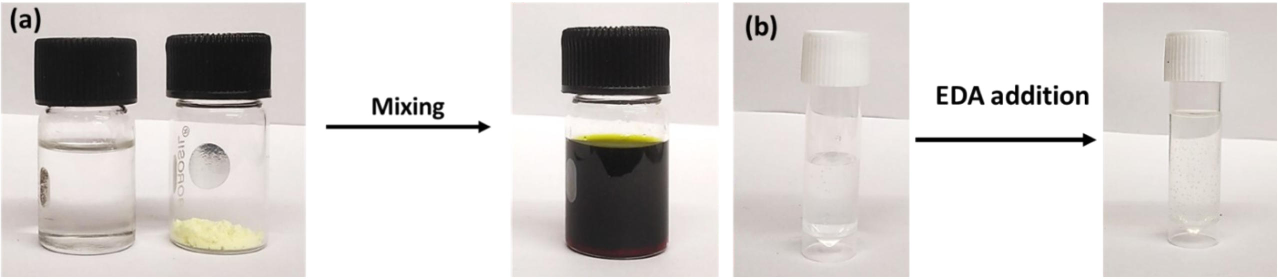

Fig. 2B (a) Photographs of sulfur and ethylene diamine before and after mixing, (b) Washed solvent before and after adding the EDA.

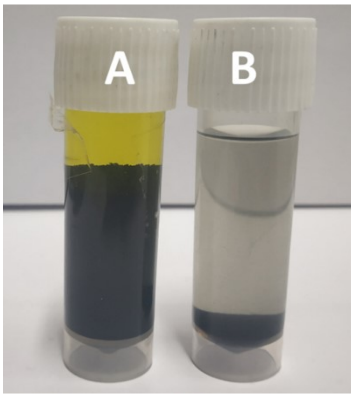

Fig. S2C. Photographs of (A) $CoFeS_2$(3:1) along with the solvent retrieved after the hydrothermal reaction, (B) $CoFeS_2$(3:1) after washing with EDA.

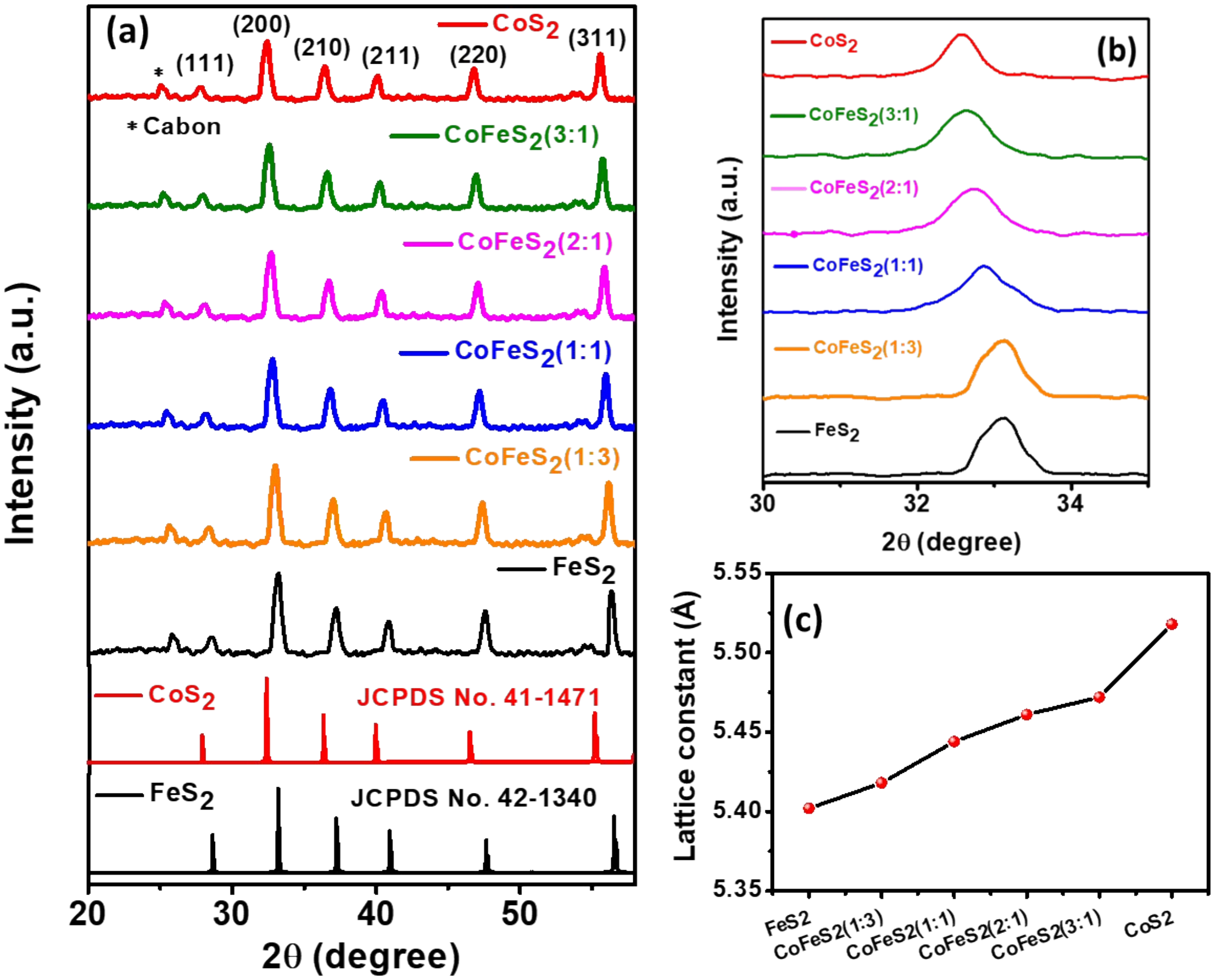

Fig. S3. (a),(b) XRD pattern of various catalysts and, (c) corresponding average lattice constant of different catalysts.

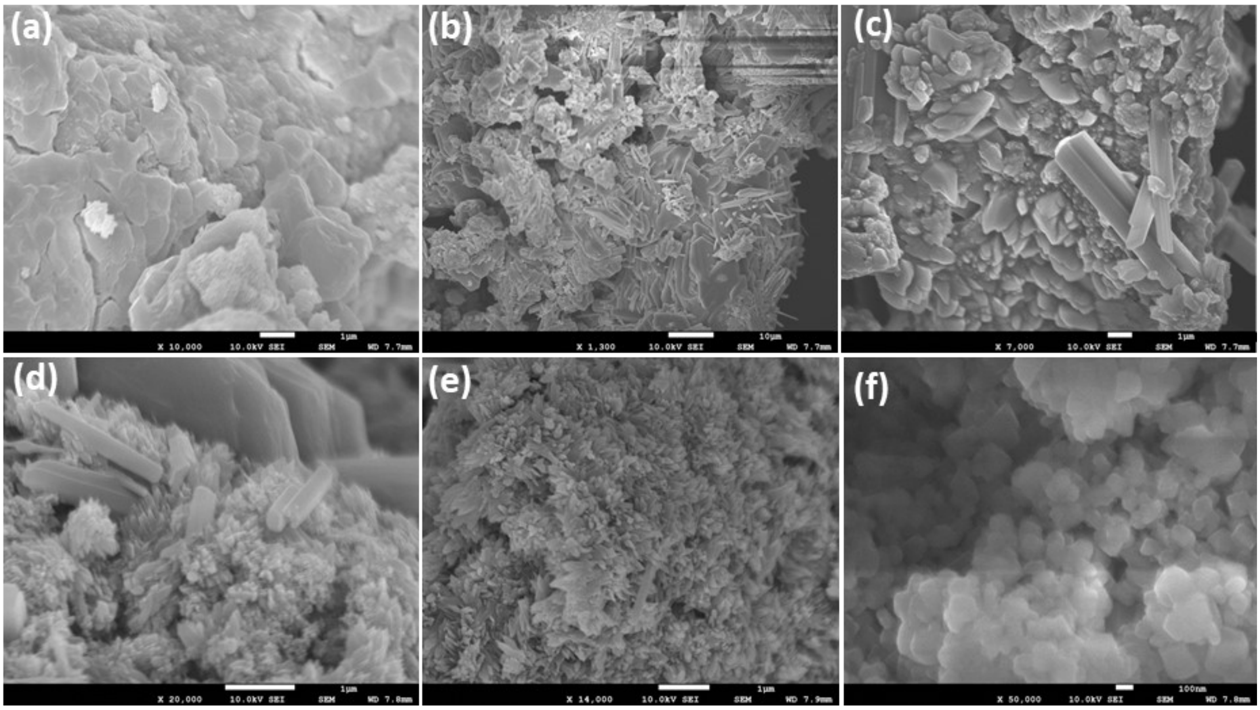

Fig. S4. FE-SEM images of (a) FeS_2, (b) $CoFeS_2$(1:3), (c) $CoFeS_2$(1:1), (d) $CoFeS_2$(2:1), (e) $CoFeS_2$(3:1) and (f) CoS_2.

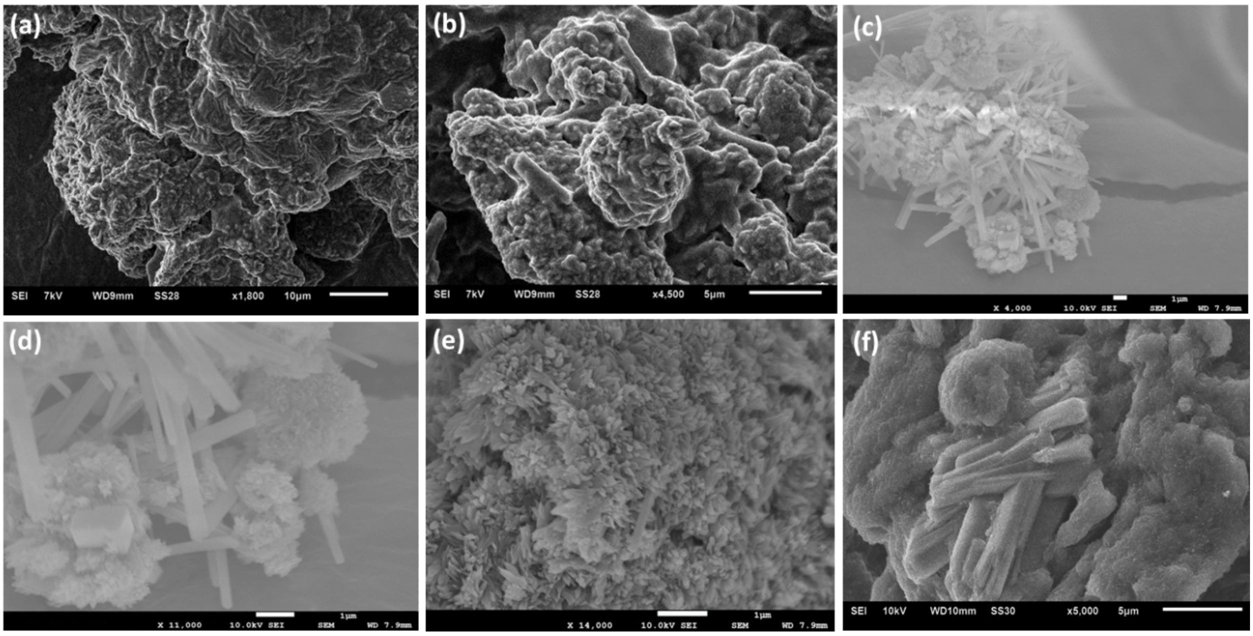

Fig. S5. SEM images of $CoFeS_2$(3:1) synthesized after (a) 2 h, (b) 4 h, (c) 8 h, (d) 10 h (e)12 h and (f) 18 h of hydrothermal reaction time.

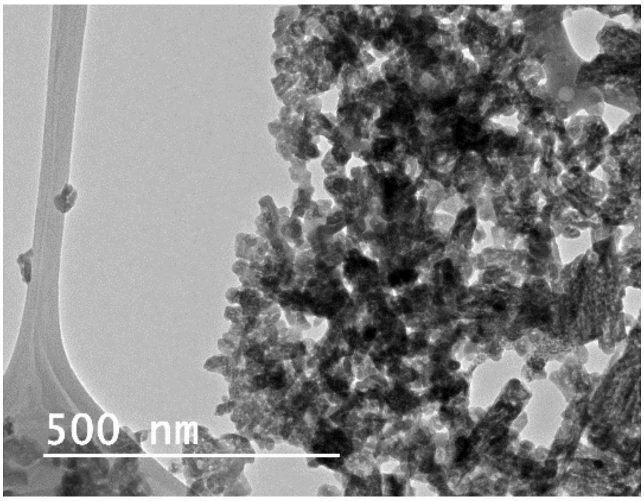

Fig. S6. TEM image of $CoFeS_2$(3:1) catalyst.

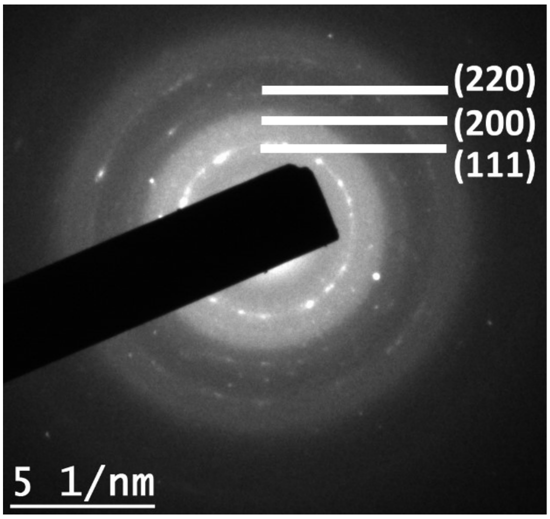

Fig. S7. SAED pattern of $CoFeS_2$(3:1) catalyst.

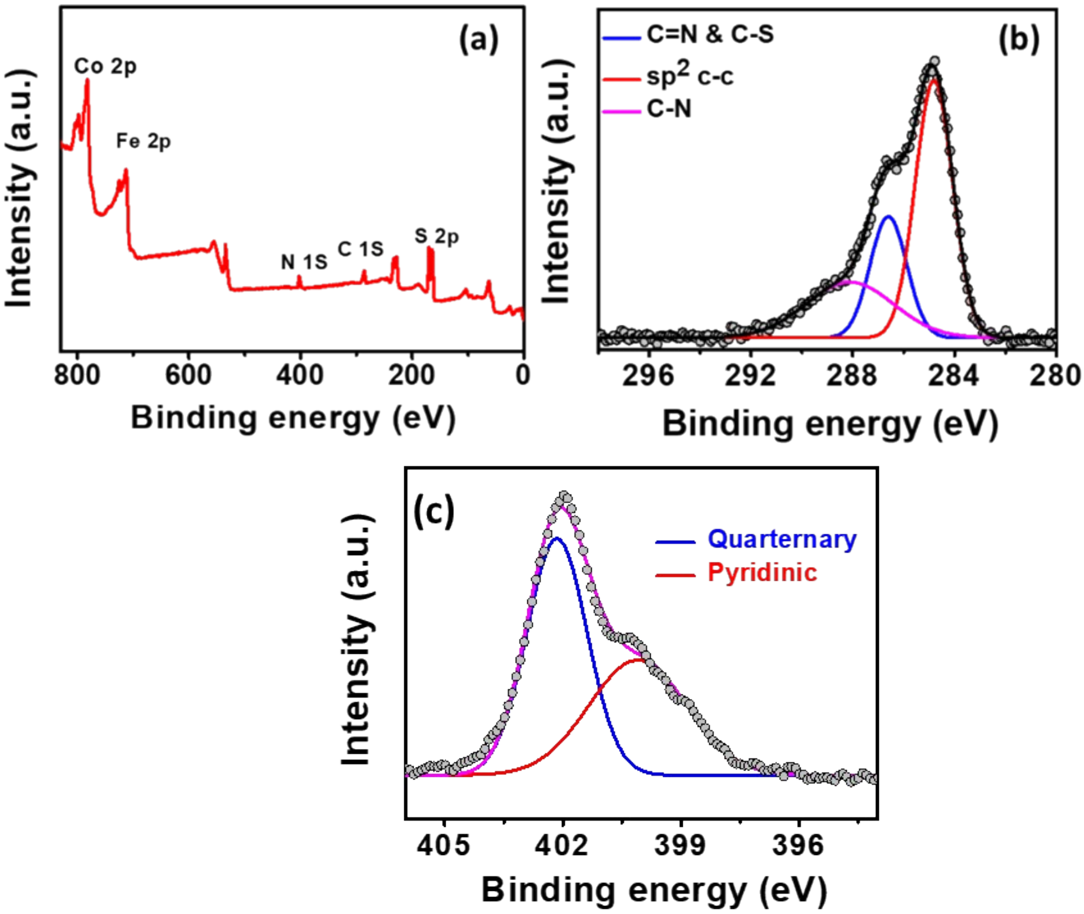

Fig. S8. (a) XPS survey spectra and deconvoluted XP spectra of (b) C 1s, and (c) N 1s, of $CoFeS_2$(3:1).

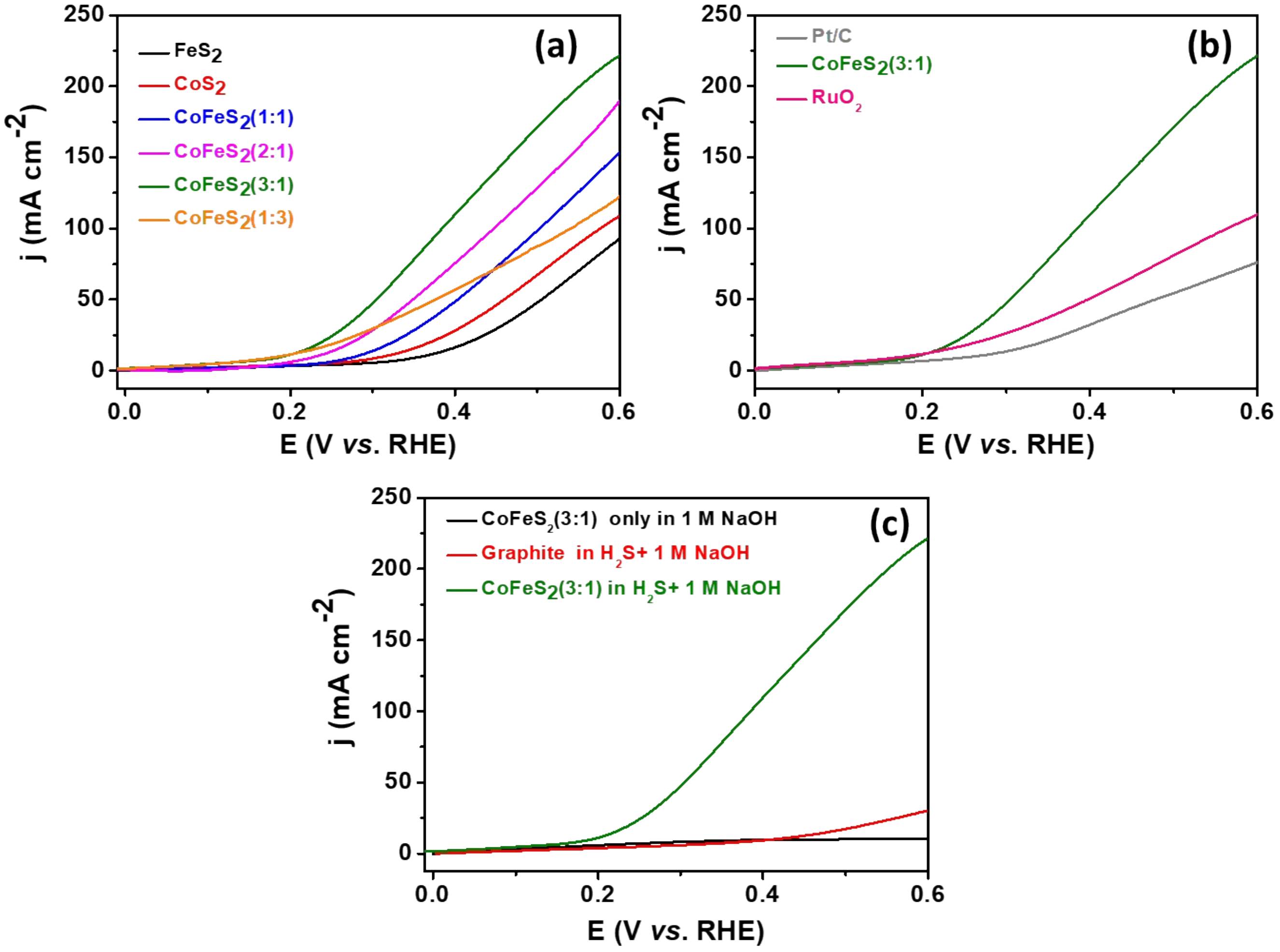

Fig. S9. Linear sweep voltammograms of (a) various catalysts, (b) $CoFeS_2$(3:1) with benchmark catalysts, and (c) demonstrating SOR activity of various catalysts in a H_2S saturated 1 M NaOH (stirred @ 600 rpm) at a scan rate of 5 mV s^{-1}, CE: graphite rod, RE: Hg/HgO/1 M NaOH.

Oxygen evolution reaction (OER activity):

The OER activity of all the catalysts was assessed in 1 M NaOH using a three-electrode assembly. Wherein catalyst coated glassy carbon electrode (GCE, Ø 2 mm) act as working electrode (WE), Pt wire counter electrode, and Hg/HgO/1 M NaOH as reference electrode respectively. The LSVs were recorded at 5 mV s^{-1} over the potential range of 1.2 V to 1.685 V *vs.* RHE. As shown in Fig. S10 for $CoFeS_2$(3:1), current density remains almost the same when LSV was scanned from 1.2 to 1.47 V, but with further increase in potential, a steep increase in the current density corresponds to the OER, which is further evidenced by the evolution of oxygen bubbles on the electrode surface. Among all the catalysts, $CoFeS_2$(3:1) shows the lowest onset and higher current density showing the enhanced activity of $CoFeS_2$(3:1) for OER.

Furter to determine the stability of the catalyst, a constant potential was imposed on the WE @1.55 V *vs.* RHE for 30 h. As shown in Fig. S10b, the same current density was maintained, confirming the stability of the catalyst at high potentials during OER.

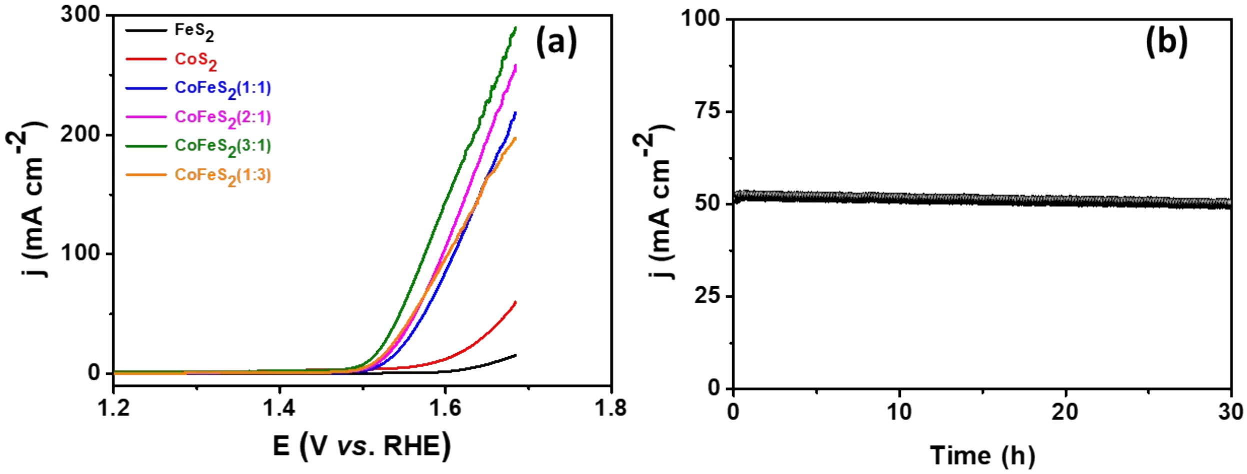

Fig. S10. Linear sweep voltammograms of various catalysts at a scan rate of 5 mV s^{-1} for OER, (b) chronoamperometry curve for $CoFeS_2$(3:1) @ 1.55 V vs. RHE in 1 M NaOH (stirred @ 600 rpm), CE: graphite rod , RE: Hg/HgO/1 M NaOH.

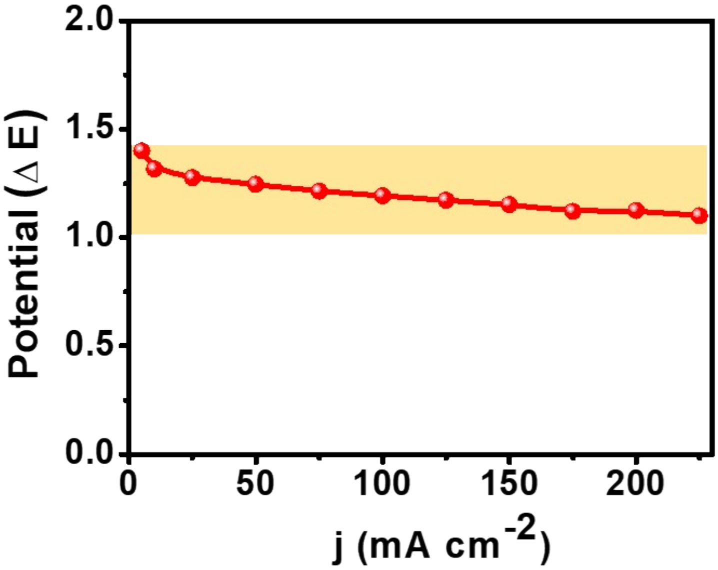

Fig. S11. The potential difference comparison of SOR and OER for $CoFeS_2$(3:1) at different current densities ranging from 5-225 mA cm^{-2} (stirred electrolyte @ 600 rpm).

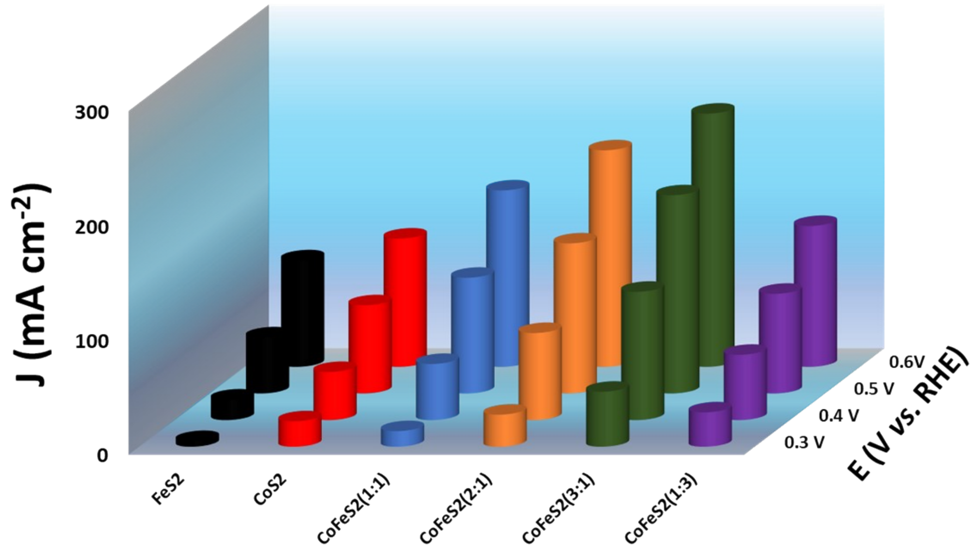

Fig. S12. Bar diagram representing current densities obtained for various catalysts at different potentials for SOR in a H_2S saturated 1 M NaOH (stirred @ 600 rpm) at a scan rate of 5 mV s^{-1}, CE: graphite rod, RE: Hg/HgO/1 M NaOH.

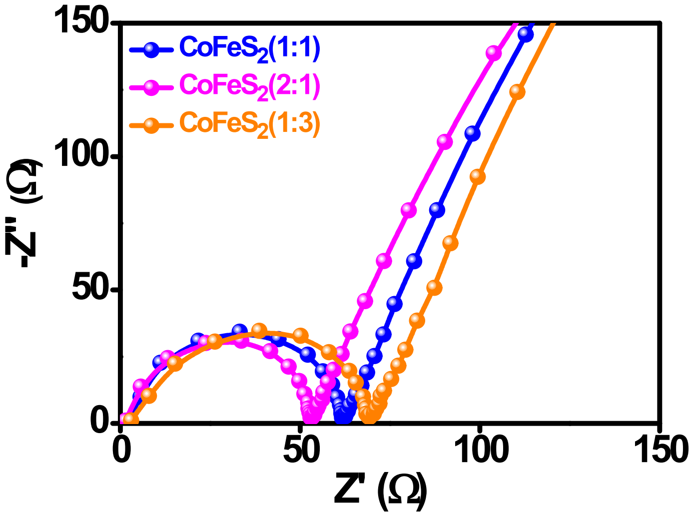

Fig. S13. EIS of various catalysts in a H_2S saturated 1 M NaOH, CE: graphite rod, RE: Hg/HgO/1 M NaOH.

Table S1: Electrochemical Impedance analysis extracted from Fig. 2d and S13.

Catalysts	R1(Solution resistance)	R2(Polarization resistance)	R_{ct} = R2-R1
FeS_2	5.64	77.0	71.36
CoS_2	4.01	72.66	68.65
$CoFeS_2$(1:1)	2.02	60.1	58.08
$CoFeS_2$(2:1)	1.48	53.2	51.72
$CoFeS_2$(3:1)	1.0	46.92	45.92
$CoFeS_2$(1:3)	3.011	69.02	66.01

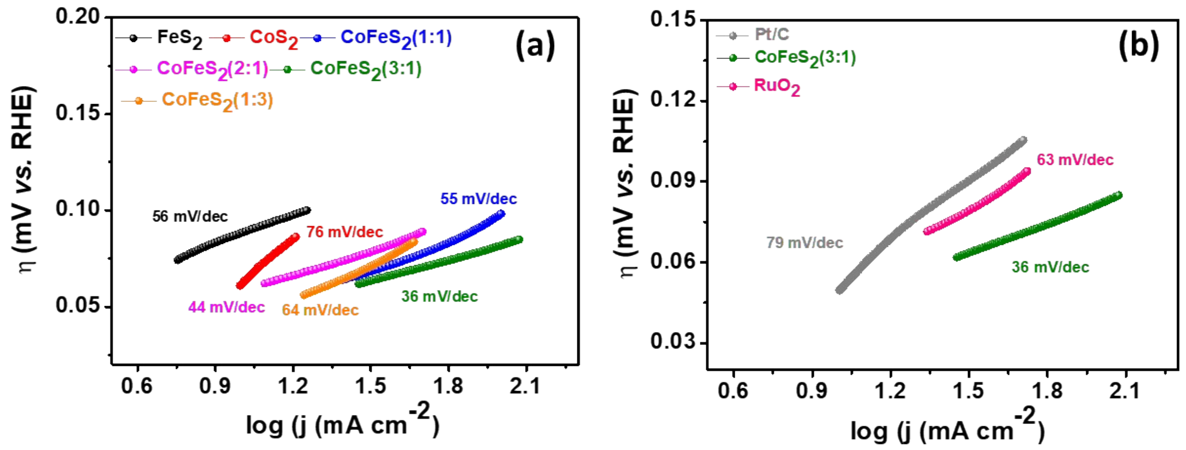

Fig. S14. (a), (b) are Tafel plots for various catalysts extracted from Fig. 2a (main manuscript) in a H_2S saturated 1 M NaOH, CE: graphite rod, RE: Hg/HgO/1 M NaOH.

Electrochemical surface area (ECSA):

To uncover the superior performance of the catalyst towards SOR, ECSA is a vital tool that directly influenced catalyst performance due to its closed relation with the no. of active sites. ECSA calculated from double-layer capacitance C_{dl}, for that initially CV was recorded at various scan rate ranging from 10-100 mV s^{-1} in the non-faradaic region from 0.0 V to 0.15 V *vs.* RHE in a H_2S saturated 1 M NaOH. The plot of the average current density $((I_a+I_c)/2)$ *vs.* scan rate gives us the double-layer capacitance. ECSA is calculated by dividing this slope with specific capacitance (20-60 μF cm^{-2}) of the flat standard surface in the present study and its value is considered to be 40 μF cm^{-2}. [1] The obtained results clearly indicate that ECSA was drastically enhanced for binary CoFe based catalysts. The ECSA for $CoFeS_2$(3:1) is 10.76 $cm^{2,}$ which is higher than all other catalysts (detailed in Table S1).

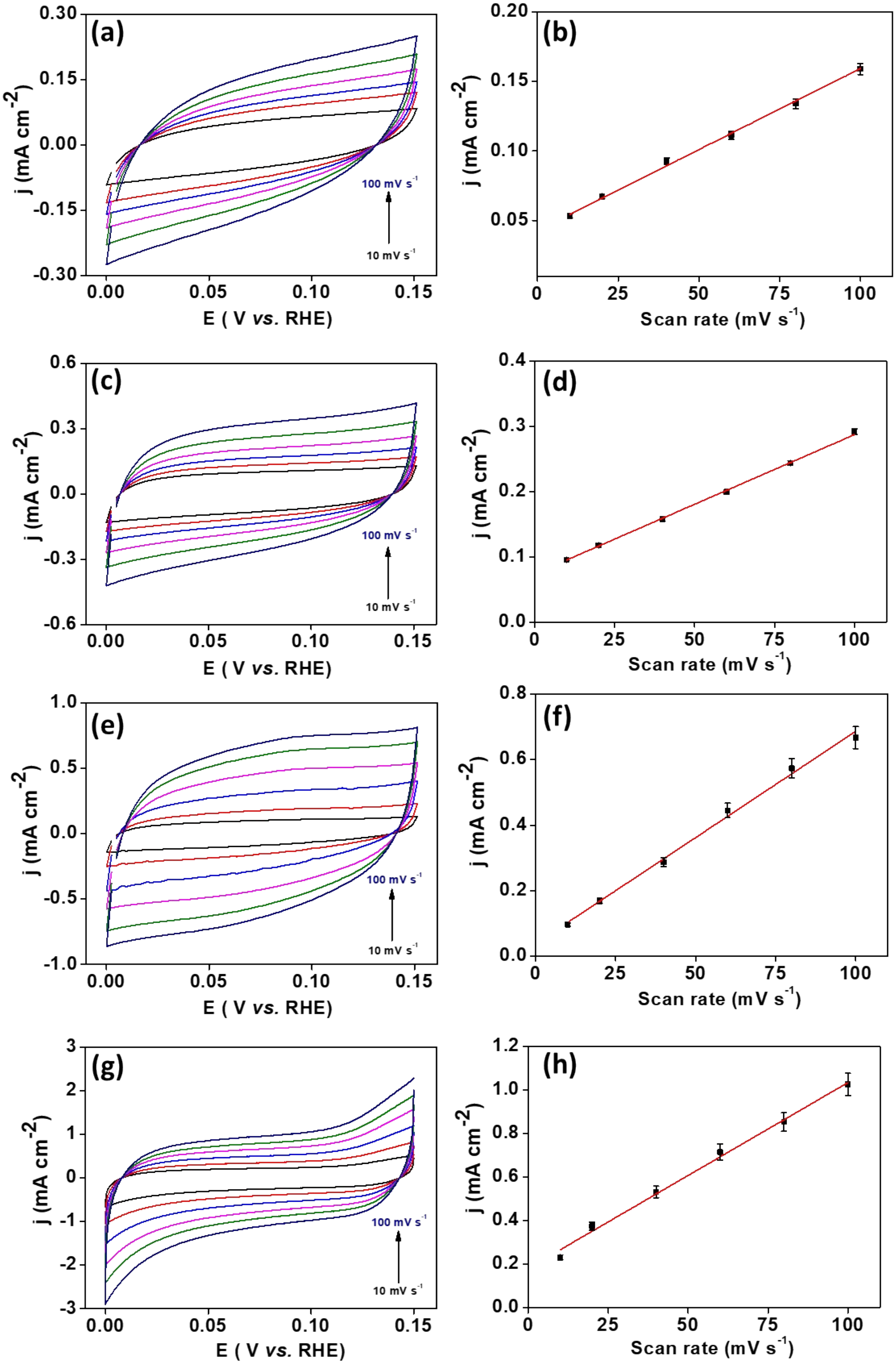
(a)
j (mA cm^{-2})
0.30
0.15
0.00
-0.15
-0.30
0.00
0.05
0.10
0.15
E (V vs. RHE)
100 mV s^{-1}
10 mV s^{-1}
(b)
j (mA cm^{-2})
0.20
0.15
0.10
0.05
0
25
50
75
100
Scan rate (mV s^{-1})
(c)
j (mA cm^{-2})
0.6
0.3
0.0
-0.3
-0.6
0.00
0.05
0.10
0.15
E (V vs. RHE)
100 mV s^{-1}
10 mV s^{-1}
(d)
j (mA cm^{-2})
0.4
0.3
0.2
0.1
0.0
0
25
50
75
100
Scan rate (mV s^{-1})
(e)
j (mA cm^{-2})
1.0
0.5
0.0
-0.5
-1.0
0.00
0.05
0.10
0.15
E (V vs. RHE)
100 mV s^{-1}
10 mV s^{-1}
(f)
j (mA cm^{-2})
0.8
0.6
0.4
0.2
0.0
0
25
50
75
100
Scan rate (mV s^{-1})
(g)
j (mA cm^{-2})
3
2
1
0
-1
-2
-3
0.00
0.05
0.10
0.15
E (V vs. RHE)
100 mV s^{-1}
10 mV s^{-1}
(h)
j (mA cm^{-2})
1.2
1.0
0.8
0.6
0.4
0.2
0.0
0
25
50
75
100
Scan rate (mV s^{-1})

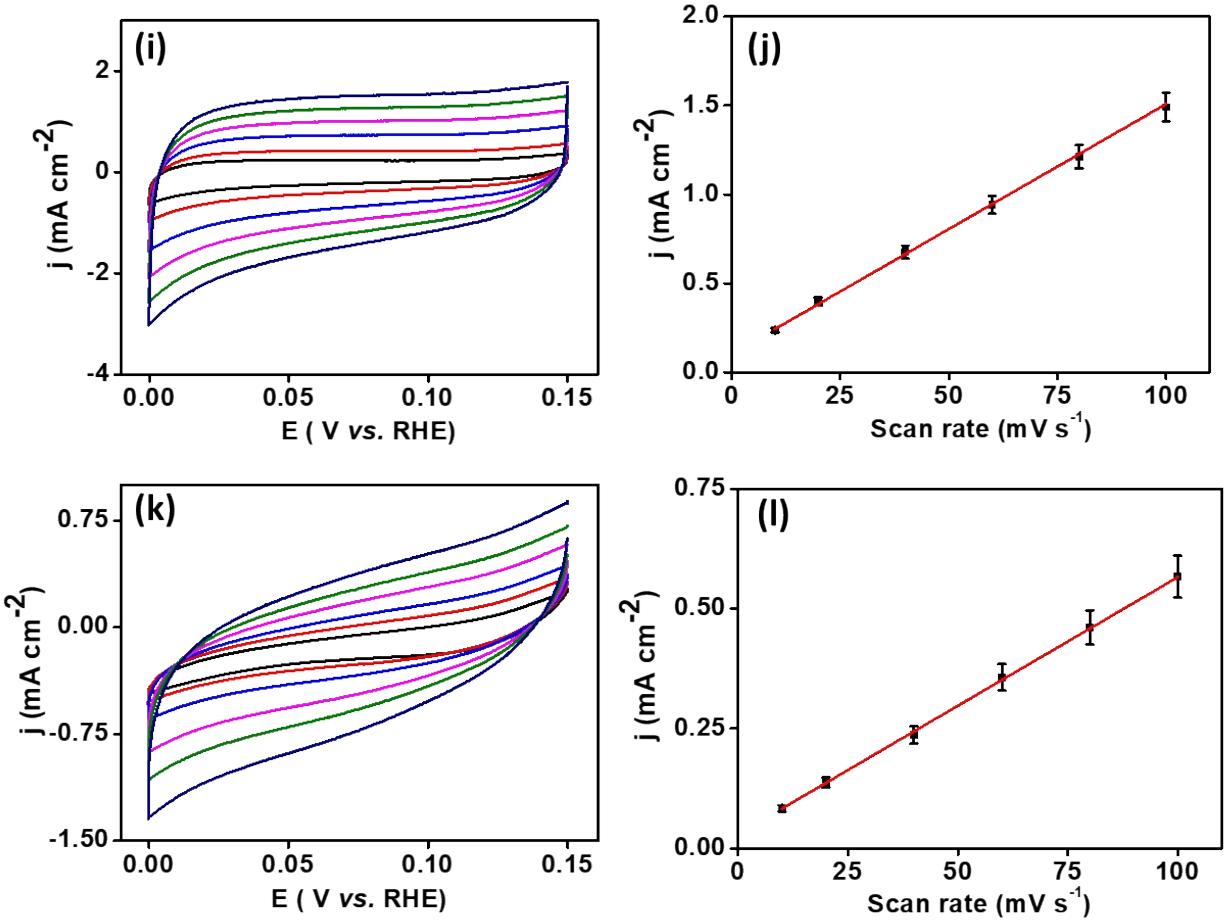

Fig. S15. Cyclic voltammograms of (a) FeS_2, (c) CoS_2, (e) $CoFeS_2$(1:1), (g) $CoFeS_2$(2:1) (i) $CoFeS_2$(3:1), (k) $CoFeS_2$(1:3) at various scan rates in the non-faradaic potential region and (b), (d), (f), (h), (j), (l) are corresponding average current versus scan rate plot in a H_2S saturated 1 M NaOH, CE: graphite rod , RE: Hg/HgO/1 M NaOH.

Table S2: Electrochemical surface area (ECSA) of various catalysts.

Catalyst	**C_{dl}^* (mF) at -0.075 V *vs.* RHE**	**ECSA (cm^2)**
FeS_2	35.98	0.9
CoS_2	68	1.70
$CoFeS_2$(1:1)	203.8	5.09
$CoFeS_2$(2:1)	261.8	6.54
$CoFeS_2$(3:1)	435.6	10.89
$CoFeS_2$(1:3)	169.6	4.24

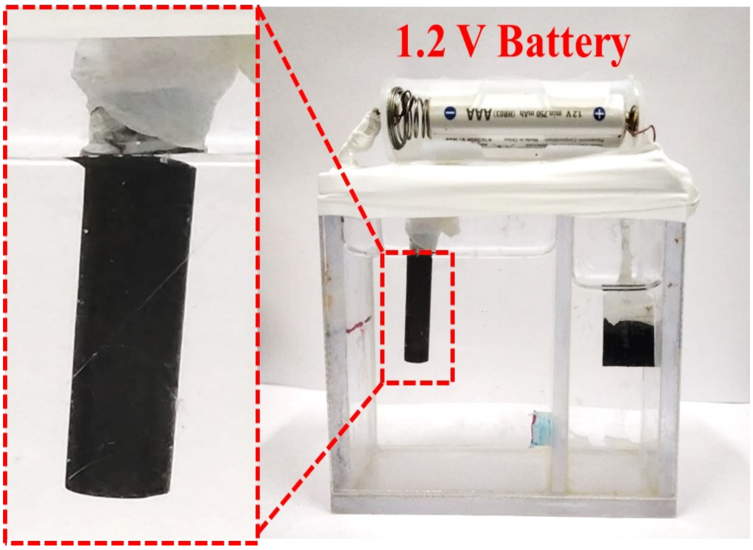

Fig. S16. Photograph of a device with 1.2 V commercial battery unable to carry out water splitting in 1 M NaOH and enlargement in the red block showing the image of the counter electrode.

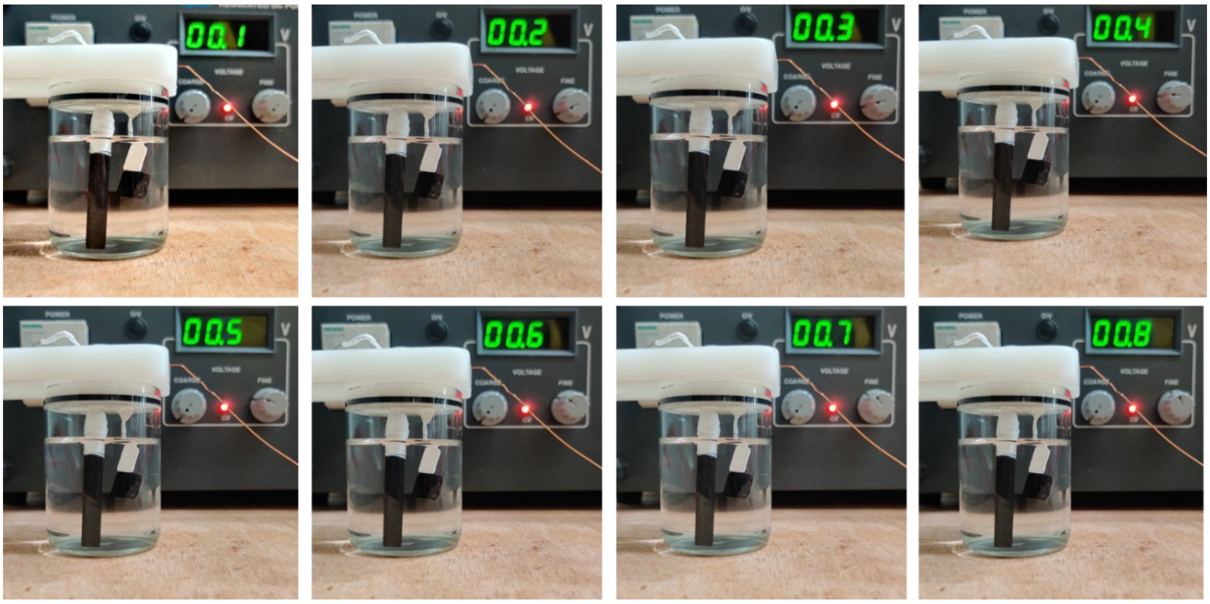

Fig. S17. Photographic images of the device constructed in the undividable cell to drive splitting of H_2O in 1 M NaOH at different potentials, using $CoFeS_2$(3:1) coated graphite paper working electrode and graphite counter electrode.

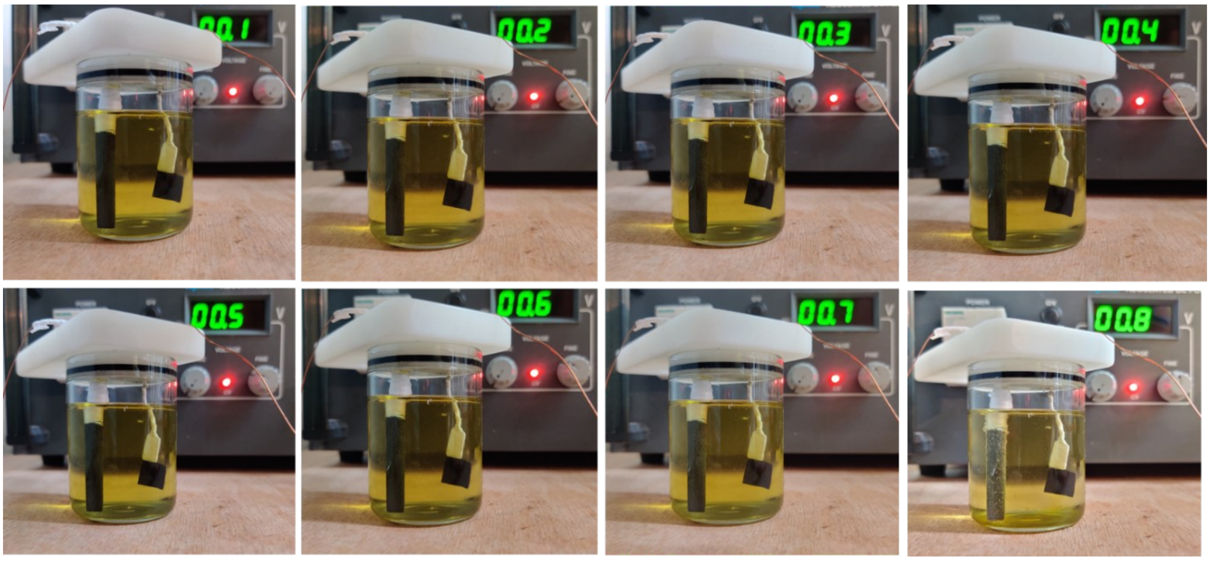

Fig. S18. Photographic images of the device constructed in the undividable cell to drive splitting of H_2S in a H_2S saturated 1 M NaOH at different potentials, using $CoFeS_2$(3:1) coated graphite paper working electrode and graphite counter electrode.

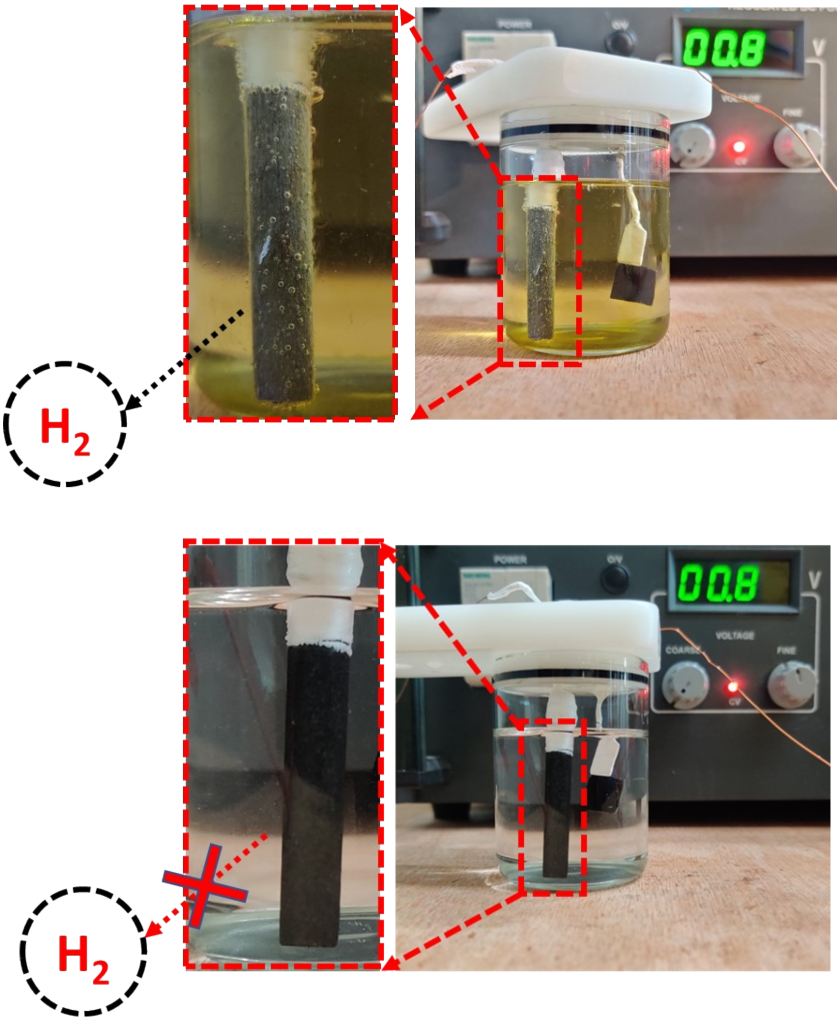

Fig. S19. Photographs of a device constructed to drive electrochemical splitting of H_2S (top) in a H_2S saturated 1 M NaOH and H_2O (bottom) in 1 M NaOH at 0.8 V direct potential using $CoFeS_2$(3:1) coated graphite paper working electrode and graphite counter electrode.

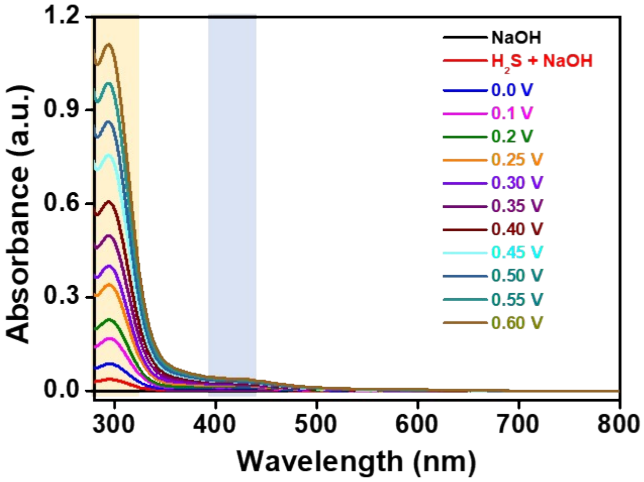

Fig. S20. In-situ UV-Vis spectra of the electrolyte recorded at various potentials during sequential chronoamperometric study.

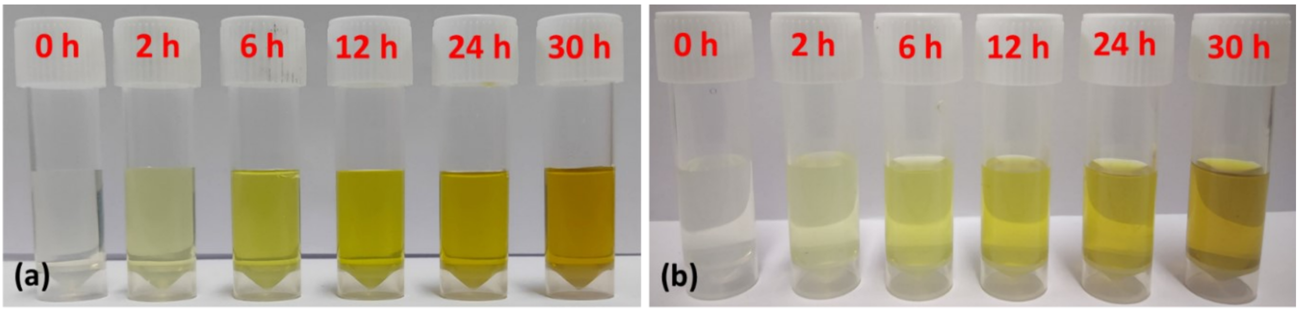

Fig. S21. (a) Photographic image of the electrolyte retrieved from chronoamperometric measurement during stability studies at different time intervals and (b) no changes in the colour of the electrolyte even after two days.

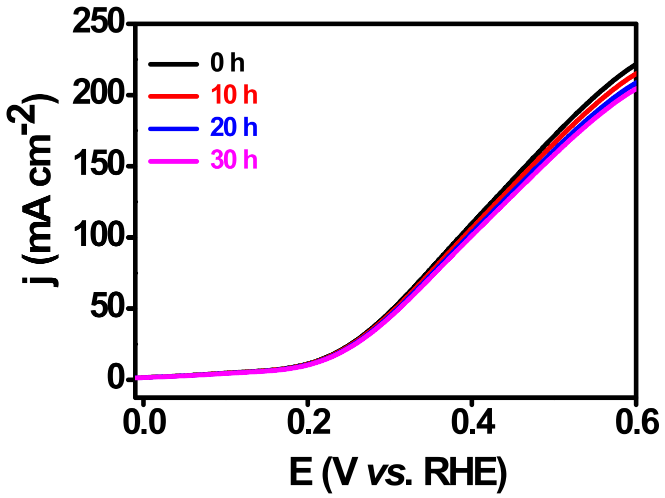

Fig. S22. LSVs for $CoFeS_2$(3:1) at 5 mV s^{-1} after different intervals of time during stability test at 0.3 V *vs.* RHE for 30 h.

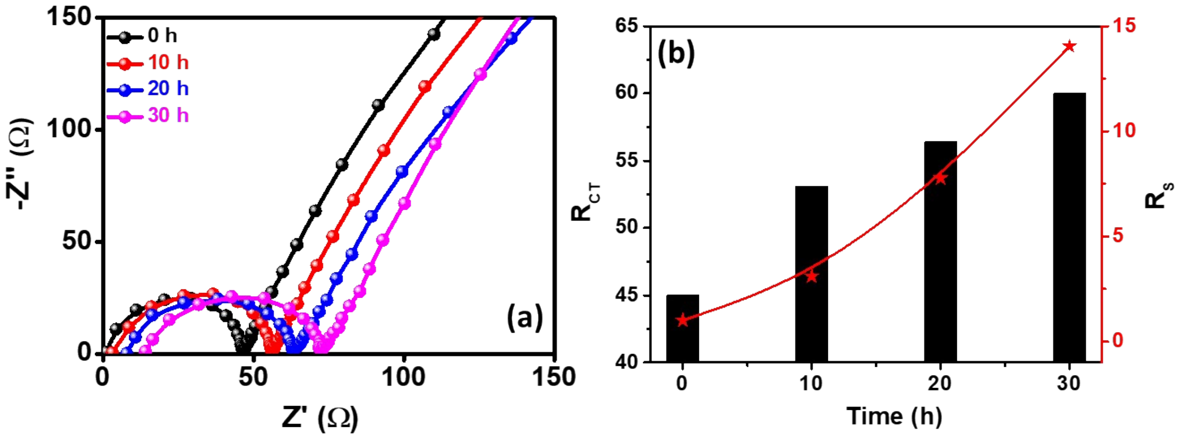

Fig. S23. (a) EIS of $CoFeS_2$(3:1) and (b) corresponding solution resistance and charge transfer resistance measured at different time intervals during the chronoamperometric stability test in a H_2S saturated 1 M NaOH, CE: graphite rod RE: Hg/HgO/1 M NaOH.

During the stability the electrolyte becomes more viscous and darker yellow with increased time of polarization (Fig. S21). Hence further experiments were continued by replacing the previous electrolyte with a fresh electrolyte after every 30 h of electrolysis. More importantly, the current density remains almost constant in the time scale of hrs even after 120 h, demonstrating the high stability of the catalyst well complemented by a negligible change in onset and current density for the LSVs recorded for $CoFeS_2$(3:1) after different interval of time

(Fig. S22). Further, EIS showed a minor increase in both solution resistance and charge transfer due to increased viscosity during the reaction (Fig. S23).

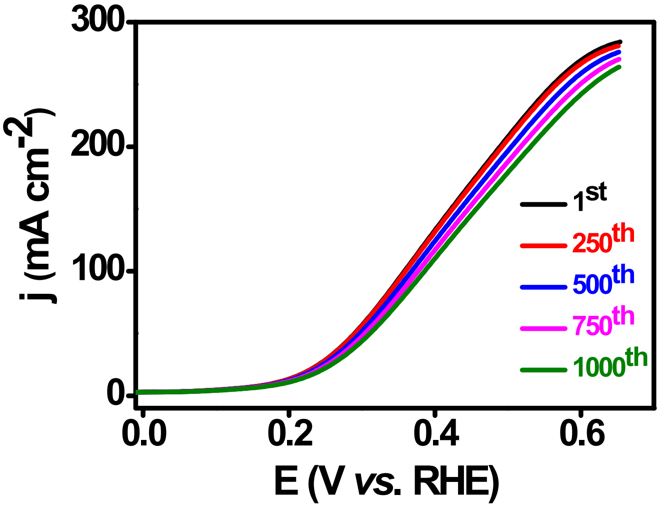

Fig. S24. LSVs of $CoFeS_2$(3:1) during cycling stability at a scan rate of 50 mV s^{-1} over 250 cycles in H_2S saturated 1 M NaOH (stirred @ 600 rpm).

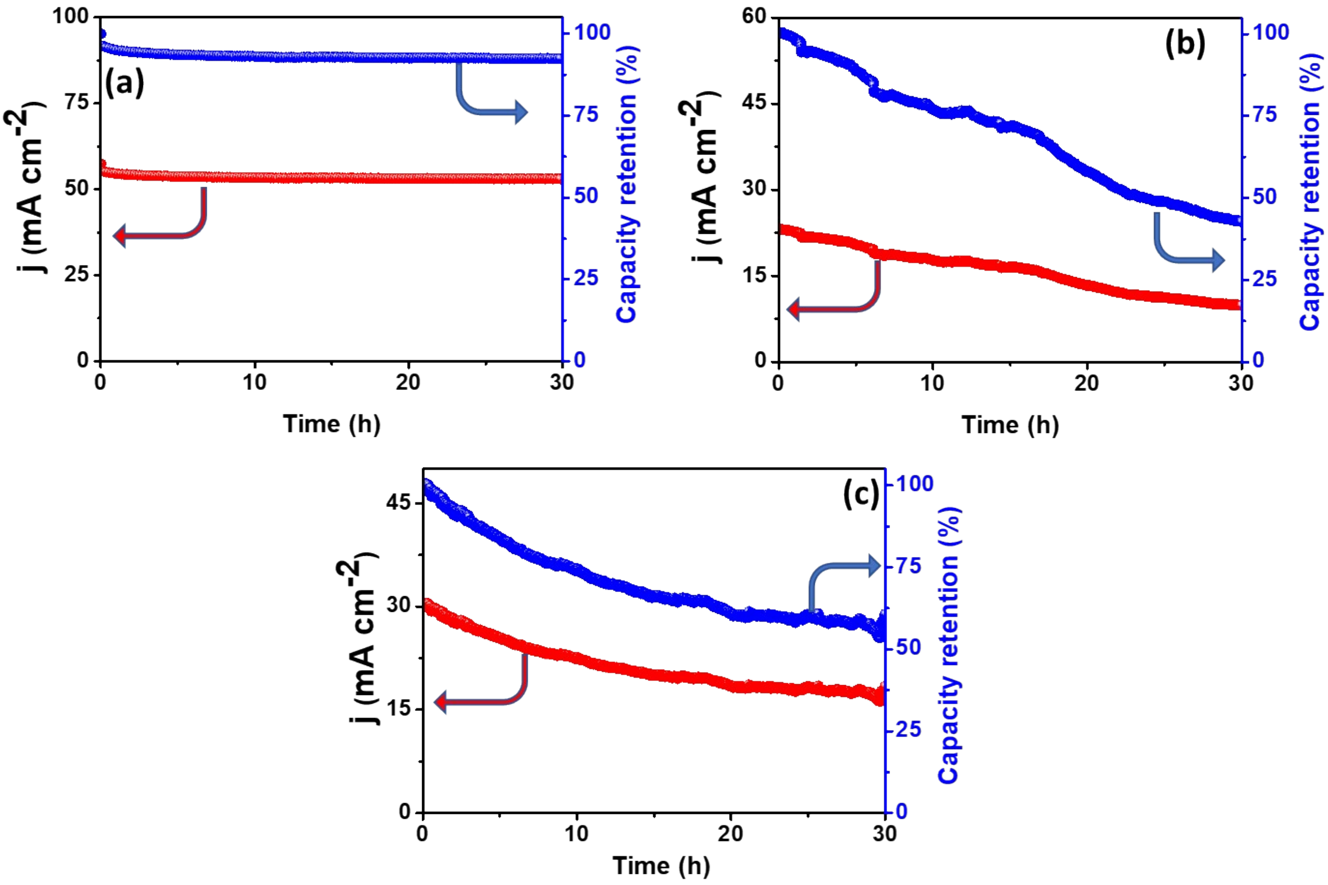

Fig. S25. Chronoamperometry stability measurements for (a) $CoFeS_2$(3:1) and (b) Pt/C for 30 h respectively at 0.3 V *vs.* RHE in a H_2S saturated 1 M NaOH, CE: graphite rod, RE: Hg/HgO/1 M NaOH.

To see whether our catalyst can survive under such conditions, we have extended the LSV to 1 V for direct S formation. As can be seen from Fig. S11, the current response decrease steadily due to the accumulation of S on the electrode surface, which is further confirmed by the appearance of sulfur peaks in the XRD. Therefore, these results indicate the importance of restricting the oxidation up to sulfide formation for extended catalysts life. We have further calculated the ECSA, which comes out to be 6.15 cm^{-2}, demonstrating that the active sites are decreased up to 56 % due to the sulfur accumulation on the electrode surface.

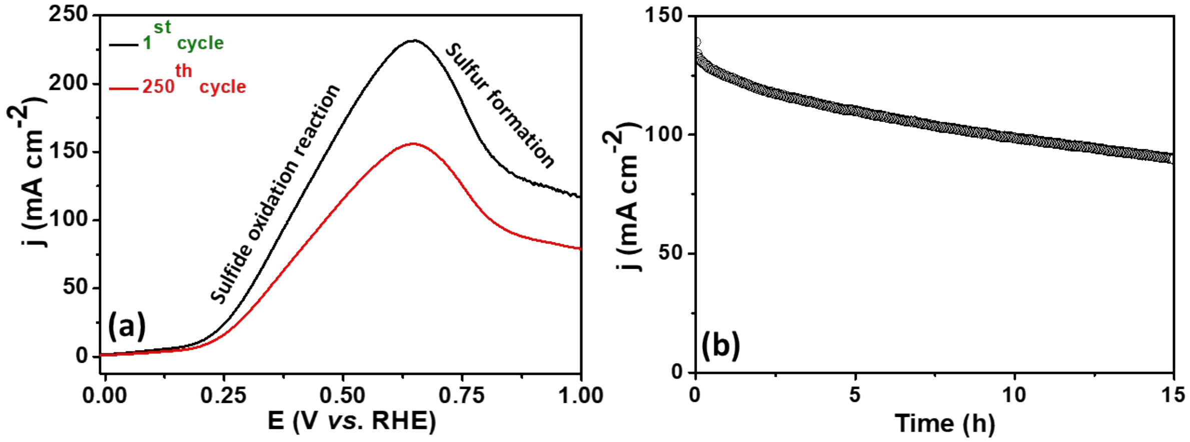

Fig. S26. Extended linear sweep voltammograms upto 1.0 V for direct Sulfur formation at a scan rate of 5 mV s^{-1}, (b) chronoamperometric curve for $CoFeS_2$(3:1) @ 0.85 V *vs.* RHE in H_2S saturated 1 M NaOH (stirred @ 600 rpm), CE: graphite rod, RE: Hg/HgO/1 M NaOH.

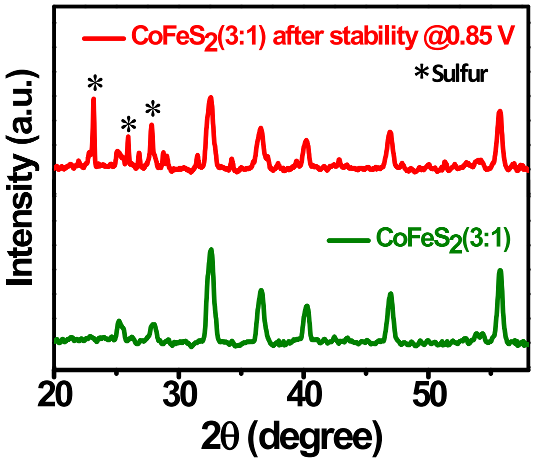

Fig. S27. XRD patterns of $CoFeS_2$(3:1) before and after stability study @ 0.85 V vs. RHE .

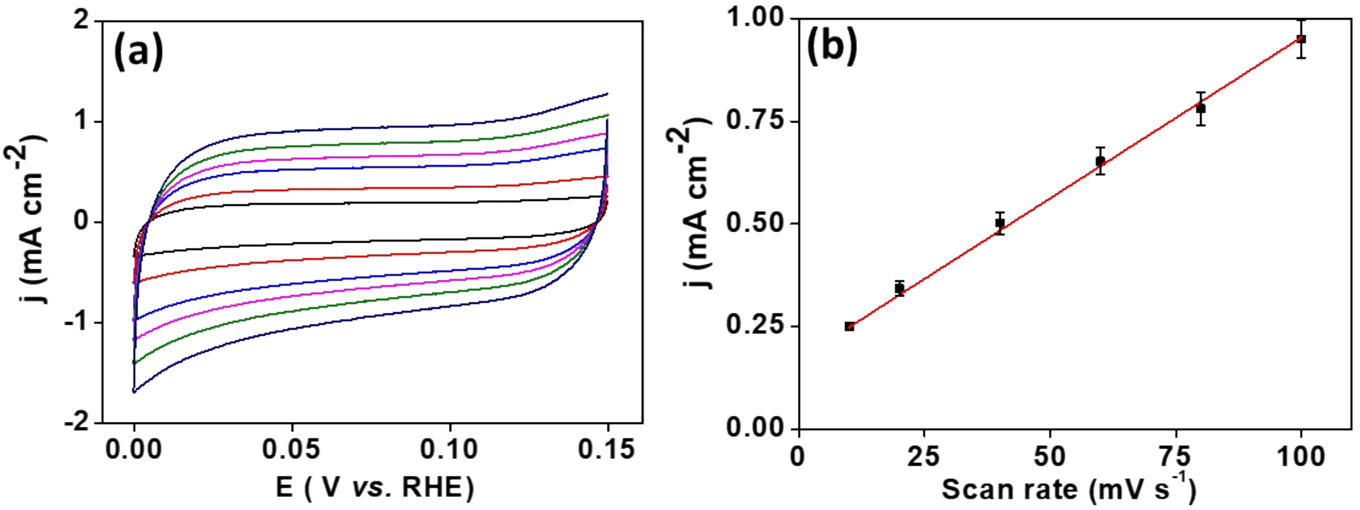

Fig. S28. (a) Cyclic voltammograms of (a) $CoFeS_2$(3:1), at various scan rates in the non-faradaic potential region and (b) are corresponding average current versus scan rate plot in an H_2S saturated 1 M NaOH after stability study @ 0.85 V for 30 h, CE: graphite rod, RE: Hg/HgO/1 M NaOH.

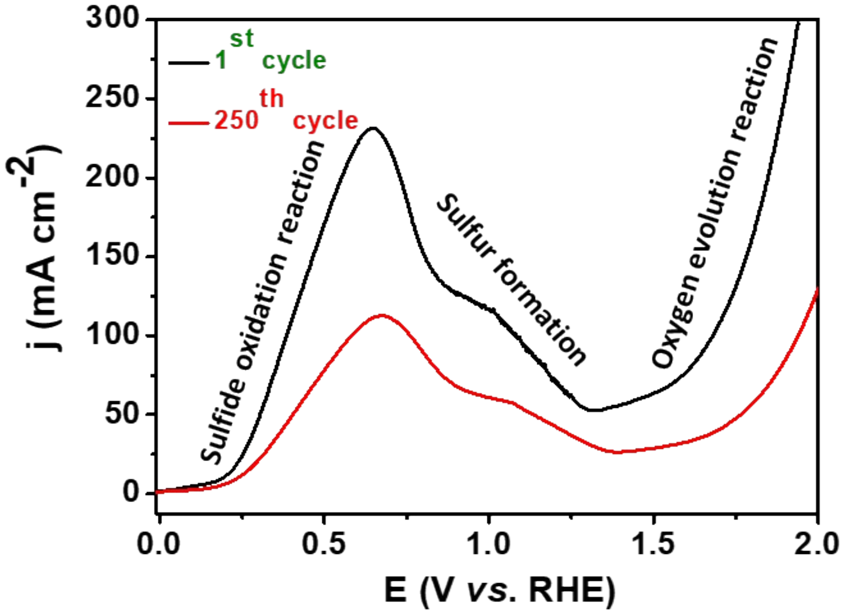

Fig. S29. Extended linear sweep voltammograms upto 2.0 V at a scan rate of 5 mV s^{-1} in H_2S saturated 1 M NaOH (stirred @ 600 rpm), CE: graphite rod, RE: Hg/HgO/1 M NaOH.

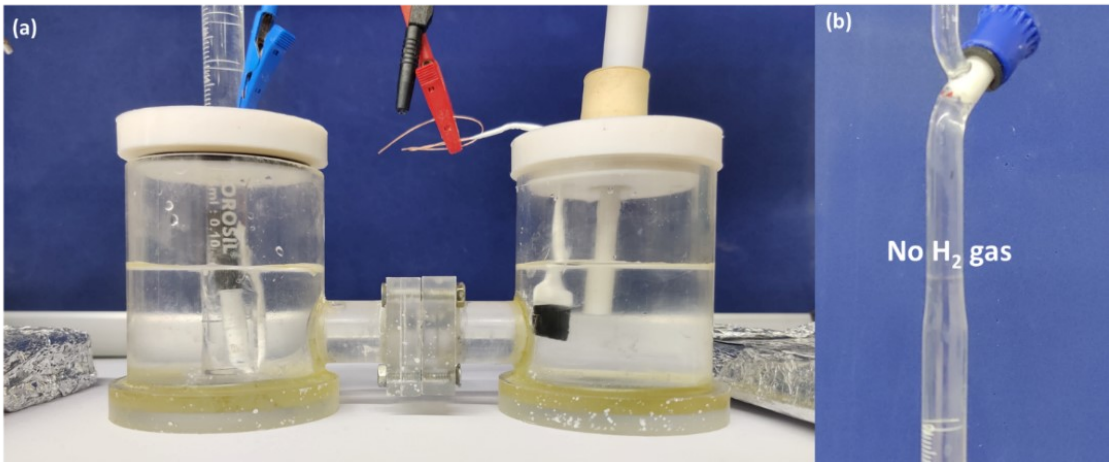

Fig. S30. (a) Photographs of the set up used for the quantification of H_2 produced during water oxidation by eudiometric method @ 0.3 V *vs.* RHE, (b) showing filling of the gas in the burette by displacement of electrolyte.

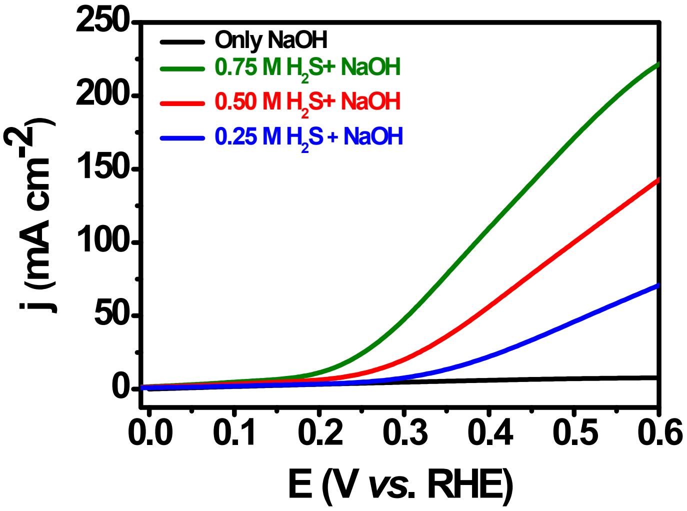

Fig. S31. LSVs for $CoFeS_2$(3:1) at 5 mV s^{-1} without H_2S and with different concentration of H_2S in 1 M NaOH (stirred @ 600 rpm), CE: graphite rod, RE: Hg/HgO/1 M NaOH.

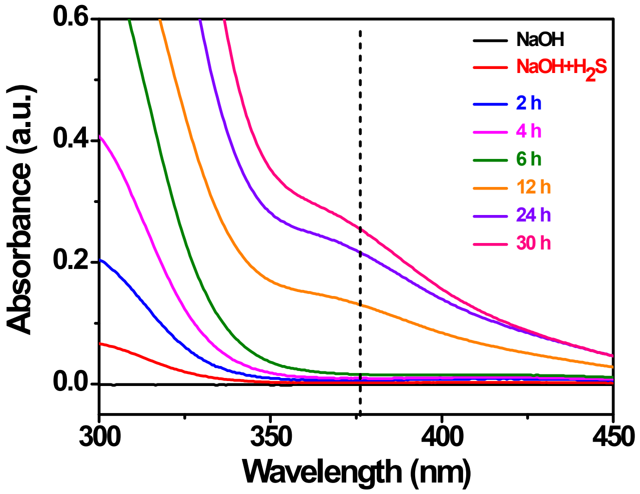

Fig. S32. Enlargement of Fig. 4e (main manuscript) showing the UV spectra of the electrolyte retrieved at various time intervals during the cycling stability.

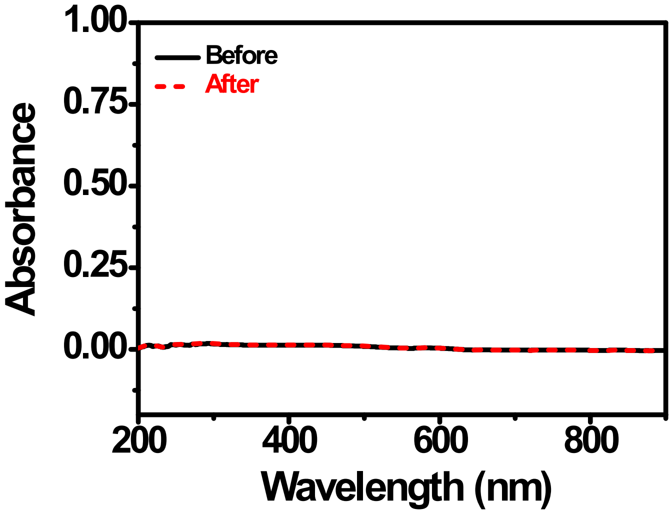

Fig. S33. UV spectra of cathodic electrolyte taken before and after stability study.

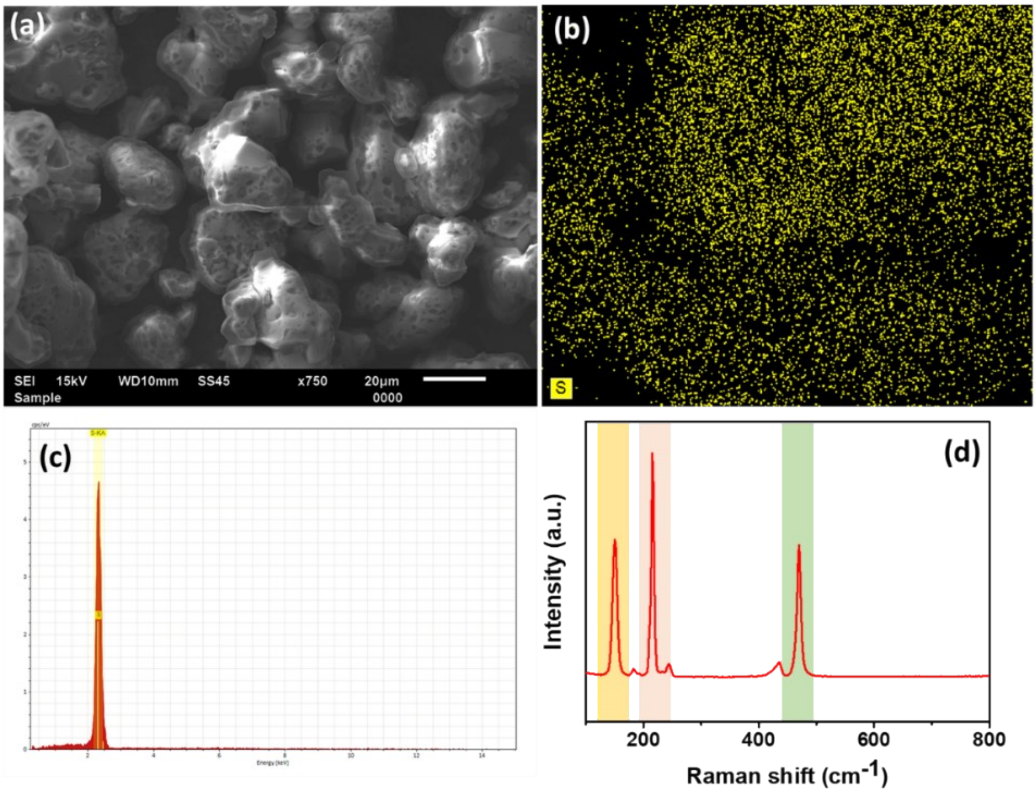

Fig. S34. (a) SEM image, (b) elemental dot mapping image, (c) EDAX and Raman spectrum of the elemental sulfur collected from polysulfide solution after acid treatment.

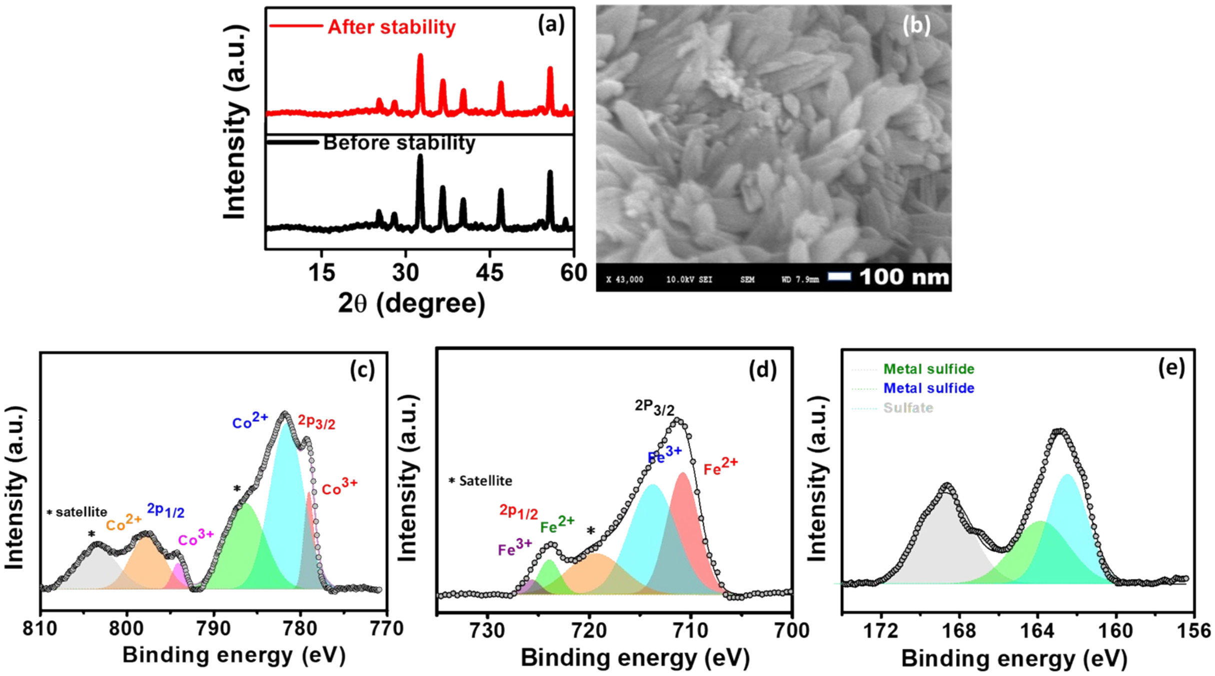

Fig. S35. (a) XRD pattern, (b) SEM image, and deconvoluted XP spectra of (c) Co 2p, (d) Fe 2p and (e) S 2p of $CoFeS_2$(3:1) after stability study at 0.3 V for 200 h in a H_2S saturated 1 M NaOH.

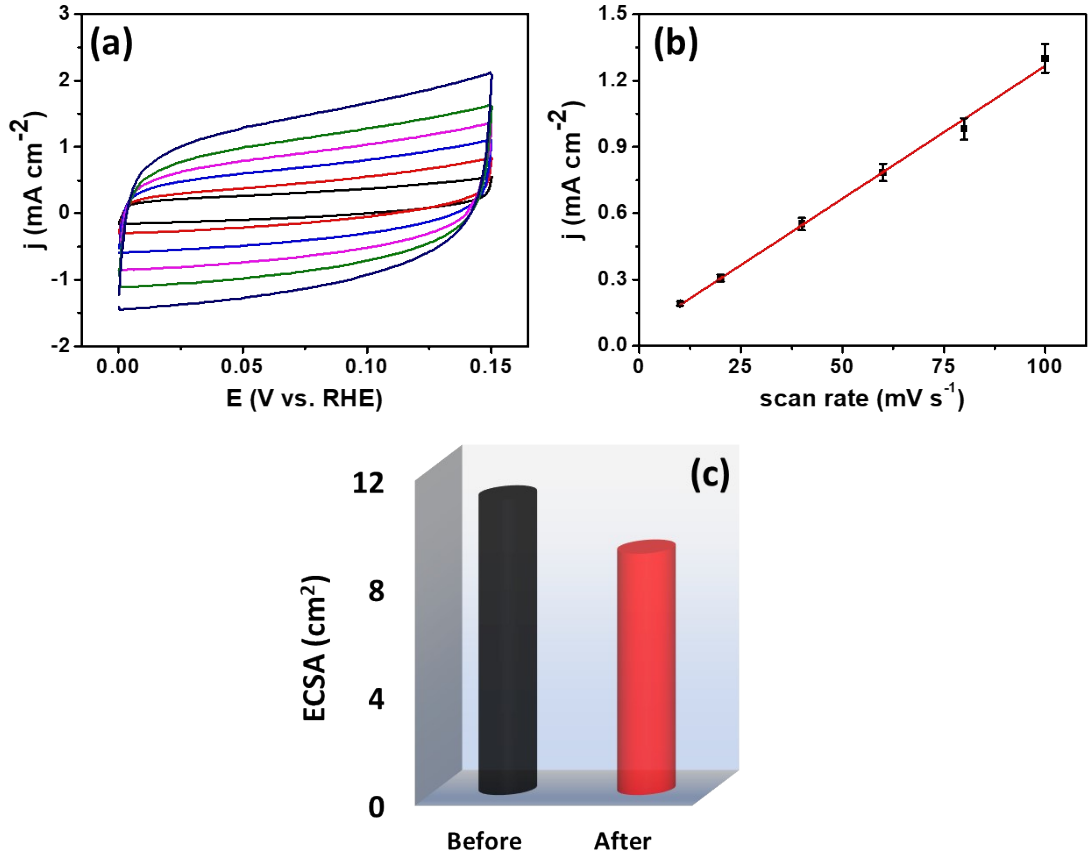

Fig. S36. Cyclic voltammograms of (a) $CoFeS_2$(3:1) after stability test at various scan rates in the non-faradaic potential region (b) corresponding average current versus scan rate plot (c) ECSA before and after the stability test in a H_2S saturated 1 M NaOH, CE: graphite rod, RE: Hg/HgO/1 M NaOH.

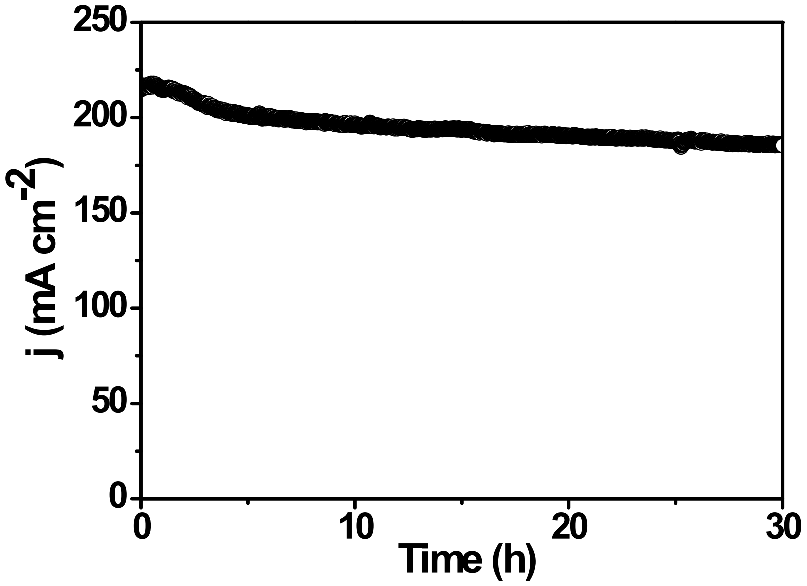

Fig. S37. (a) Chronoamperometry stability measurements for CoFeS_2(3:1) for 30 h at 0.6 V *vs.* RHE in a H_2S saturated 1 M NaOH, CE: graphite rod, RE: Hg/HgO/1 M NaOH.

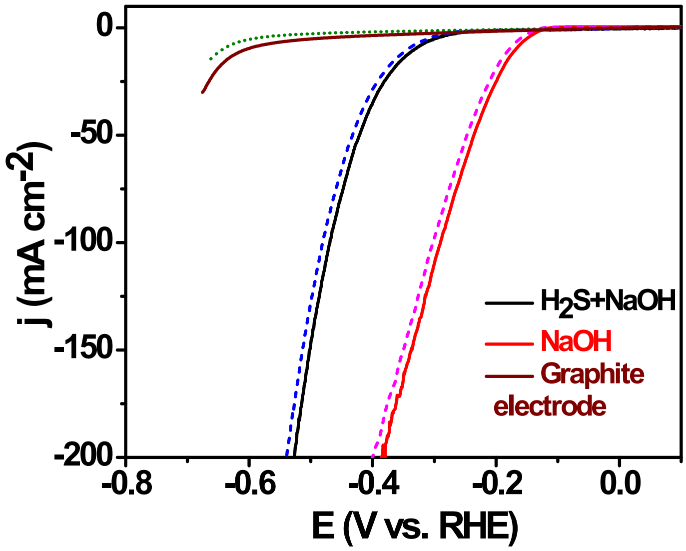

Fig. S38. LSVs showing HER activity of bare graphite electrode and CoFeS_2(3:1) at a scan rate of 5 mV s^{-1} in 1 M NaOH and H_2S saturated 1 M NaOH, CE: graphite rod, RE: Hg/HgO/1 M NaOH without and with stirring (600 rpm).

Table S3: Comparison of obtained current density for $CoFeS_2$(3:1) towards SOR with reported literature.

Catalyst	**Current density (mA cm^{-2})**		**References**
	0.3 V	**0.4 V**	
Raney Ni	0.50	1.39	**[2]**
IrO_2	1.80	6.57	**[3]**
40% Pt/C	3.31	14.73	**[3]**
CoNi@NGs	4.09	26.55	**[4]**
MoS_2	0.48	0.70	**[5]**
$CoFeS_2$(3:1) electrolyte stirred @ 600 rpm	**50**	**122**	**This Work**

Ref

erences:

1. N. Thakur, M. Kumar, S.D. Adhikary, D. Mandal, T.C. Nagaiah, PVIM–Co5POM/MNC composite as a flexible electrode for the ultrasensitive and highly selective non-enzymatic electrochemical detection of cholesterol, *Chem. Commun.*, 55 (2019) 5021-5024.
2. K. Petrov, S. Srinivasan, Low temperature removal of hydrogen sulfide from sour gas and its utilization for hydrogen and sulfur production, *Int. J. Hydrogen Energy*, 21 (1996) 163-169.
3. B. Miller, A. Chen, Effect of concentration and temperature on electrochemical oscillations during sulfide oxidation on Ti/Ta_2O_5–IrO_2 electrodes, Electrochim. Acta, 50 (2005) 2203-2212.
4. M. Zhang, J. Guan, Y. Tu, S. Chen, Y. Wang, S. Wang, L. Yu, C. Ma, D. Deng, X. Bao, Highly efficient H_2 production from H_2S via a robust graphene-encapsulated metal catalyst, Energy Environ. Sci., 13 (2020) 119-126.
5. A.E. Sanlı, A. Aytaç, M. Mat, Investigation of the electro-oxidation of artificial Black Sea water by cyclic voltammetry on molybdenum (II), Int. J. Hydrogen Energy, 39 (2014) 9221-9229.